Development/Plasticity/Repair

Altered Map of Visual Space in the Superior Colliculus of Mice Lacking Early Retinal Waves

Thomas D. Mrsic-Flogel,[1] Sonja B. Hofer,[1] Claire Creutzfeldt,[1] Isabelle Cloëz-Tayarani,[2] Jean-Pierre Changeux,[2] Tobias Bonhoeffer,[1] and Mark Hübener[1]

[1]Max-Planck-Institut für Neurobiologie, D-82152 Martinsried, Germany, and [2]Unité de Recherche Associée, Centre National de la Recherche Scientifique, D2182 Récepteurs et Cognition, Institut Pasteur, 75724 Paris Cedex 15, France

During the development of the mammalian retinocollicular projection, a coarse retinotopic map is set up by the graded distribution of axon guidance molecules. Subsequent refinement of the initially diffuse projection has been shown to depend on the spatially correlated firing of retinal ganglion cells. In this scheme, the abolition of patterned retinal activity is not expected to influence overall retinotopic organization, but this has not been investigated. We used optical imaging of intrinsic signals to visualize the complete retinotopic map in the superior colliculus (SC) of mice lacking early retinal waves, caused by the deletion of the $\beta 2$ subunit of the nicotinic acetylcholine receptor. As expected from previous anatomical studies in the SC of $\beta 2^{-/-}$ mice, regions activated by individual visual stimuli were much larger and had less sharp borders than those in wild-type mice. Importantly, however, we also found systematic distortions of the entire retinotopic map: the map of visual space was expanded anteriorly and compressed posteriorly. Thus, patterned neuronal activity in the early retina has a substantial influence on the coarse retinotopic organization of the SC.

Key words: **superior colliculus; retinal waves; retinotopic map; activity-dependent refinement; intrinsic signal imaging; $\beta 2$ subunit of nicotinic acetylcholine receptor**

Introduction

The principles of retinotopic map formation in the midbrain have been studied extensively over the past decades (Sperry, 1963; Bonhoeffer and Huf, 1982; Cline and Constantine-Paton, 1989). However, a comprehensive understanding of the mechanisms that specify the coarse retinotopic layout of the retinocollicular projection is still lacking. Whereas the initial preference of retinal ganglion cell (RGC) axons for topographically appropriate positions is mediated by axon guidance molecules (Cheng et al., 1995; Drescher et al., 1995; Frisen et al., 1998; Feldheim et al., 2000; Hindges et al., 2002), the precise topography develops during the first postnatal week by large-scale retraction of inappropriately targeted axonal branches and selective arborization within the target region (Simon and O'Leary, 1992; McLaughlin et al., 2003). This remodeling is thought to be regulated by waves of activity that sweep across the immature retina and correlate the firing of neighboring RGCs (Galli and Maffei, 1988; Meister et al., 1991; Wong et al., 1995; Bansal et al., 2000), thereby stabilizing their connections to common target neurons (Changeux and Danchin, 1976; Willshaw and von der Malsburg, 1976; Wong, 1999; Butts, 2002).

Because retinal waves are initially mediated by cholinergic (nicotinic) synaptic transmission during the first postnatal week (Bansal et al., 2000; Wong et al., 2000; Zhou and Zhao, 2000; Feller, 2002), mice deficient for the $\beta 2$ subunit of the nicotinic acetylcholine receptor (nAChR) ($\beta 2^{-/-}$ mice) (Picciotto et al., 1995; Xu et al., 1999) lack early retinal waves but maintain decorrelated spontaneous activity (McLaughlin et al., 2003). Retinofugal projections in $\beta 2^{-/-}$ mice are indeed broader than in control animals (Grubb et al., 2003), arguing strongly for correlated retinal activity being instrumental in refinement of RGC axon arborizations in target structures. Moreover, electrical recordings from LGN neurons in $\beta 2^{-/-}$ mice revealed disrupted fine-scale mapping (Grubb et al., 2003), indicating that imprecise projections bear functional consequences. Although these results made a clear case for patterned activity in the regional refinement of retinofugal projections, they did not demonstrate whether the disruption of retinal waves influences the coarse layout of the retinotopic map. If the retinotopic preference of RGC axons is predominantly specified by molecular cues, it is expected that the abolition of retinal waves during the remodeling period would result in an expansion of RGC axon arborizations without a significant perturbation of gross retinotopy.

To understand how the lack of retinal waves affects the overall retinotopic organization in target areas requires the complete visualization of the retinotopic map, which was not possible in previous studies. We used optical imaging of intrinsic signals

Received April 20, 2005; revised June 11, 2005; accepted June 16, 2005.

This work was supported by the Max Planck Society (T.D.M.F., S.B.H., C.C., T.B., M.H.) and the Humboldt Foundation (T.D.M.F.), as well as Collège de France, Association pour la Recherche sur le Cancer, Ministère de la Recherche et des Nouvelles Technologies, and Commission of the European Communities (I.C.T., J.P.C.). We thank P. Vanderhaeghen, F. Sengpiel, K. Tomita, and U. V. Nägerl for insightful comments on this manuscript and M. Sperling for help with programming.

Correspondence should be addressed to either Mark Hübener or Thomas D. Mrsic-Flogel, Max-Planck-Institut für Neurobiologie, Am Klopferspitz 18, D-82152 Martinsried, Germany. E-mail: mark@neuro.mpg.de or flogel@neuro.mpg.de.

C. Creutzfeldt's present address: Department of Neurology, University of Washington, 1959 Northeast Pacific Street, Seattle, WA 98195.

DOI:10.1523/JNEUROSCI.1555-05.2005

 0270-6474/05/256921-08$15.00/0

(Grinvald et al., 1986; Bonhoeffer and Grinvald, 1996; Schuett et al., 2002; Kalatsky and Stryker, 2003; Mrsic-Flogel et al., 2003) to obtain functional retinotopic maps from the surface of the entire superior colliculus (SC). We show that visual stimuli activate much larger regions of the SC in $\beta2^{-/-}$ mice than in control animals, and that, surprisingly, coarse retinotopy is systematically altered. Our results suggest that patterned retinal activity is more influential than previously thought in establishing the retinotopic map layout.

Materials and Methods

Experiments were performed on 15 wild-type (wt) and 13 $\beta2^{-/-}$ mice (3–5 months old) (Picciotto et al., 1995) that were backcrossed at least 10 times to the C57BL/6 strain. All surgical and experimental procedures were in accordance with the guidelines of the local government and the Society for Neuroscience.

Surgery. Mice were chamber anesthetized with 2–2.5% halothane in a 1:1 mixture of N_2O/O_2 and then intubated (1.5 mm polythene tubing) and ventilated with 1.5–2% halothane in the same gaseous mixture. After affixing the ear bars, the scalp was resected, and a 3 × 4 mm craniotomy was performed over the posterior part of the left hemisphere. The left SC was exposed by careful aspiration of the overlying cortex, covered over with 2% agarose in saline, and sealed with a 10-mm-diameter coverslip (Fig. 1*A*). The skull was glued to a head bar, and the ear bars were removed to allow unobstructed vision.

Intrinsic signal imaging and visual stimulation. Details of the imaging equipment and visual stimulation were described in detail previously (Schuett et al., 2002). The SC was illuminated with 707 nm light, and images (600 ms in duration) were captured with a cooled slow-scan CCD camera (ORA 2001; Optical Imaging, Germantown, NY), focused 200–300 μm below the SC surface. During each 9 s stimulation trial, four blank frames were acquired before the 11 frames, during which visual stimuli were presented.

A monitor (Mitsubishi Pro 2020) was placed 13.5 cm from the right eye, at a 45° angle to the long body axis, covering the visual field between 0° and 108° in azimuth and −10° and 62° in elevation. Stimuli were rectangular square-wave drifting gratings (0.04 cycles/°; 2 cycles/s) that changed their orientation every 0.6 s, presented randomly at different positions in the visual field. For each animal, SC responses were initially mapped with 12 adjacent 24° stimuli (4 × 3 grid design), spanning 108° in azimuth and 72° in elevation, to ensure that subsequent test stimuli could be placed at similar visual field positions in all animals. Overall retinotopy was mapped with 24 abutting 18° stimuli (6 × 4 grid design), spanning 108° in azimuth and 72° in elevation. For comparing the spread of SC responses in wt and $\beta2^{-/-}$ mice, stimuli of five different sizes (side length, 12°, 15°, 20°, 24.5°, and 30°) were each shown at three fixed, adjacent positions (15° center spacing) within the central region of the right visual hemifield.

Image analysis. Single-position maps were computed by clipping (1.5%) and high-pass filtering blank-corrected image averages of 12–30 stimulus repetitions (for details, see Schuett et al., 2002). For each single-condition map, the patch area was determined as the area of all pixels with values ≥50% of the maximum response. The 50% response region was defined by plotting a contour line for 50% of the maximum response in Gaussian-smoothed single-position maps. The overlap between adjacent patches was calculated according to the following formula: $O = (N_o)/(N_1 + N_2 - N_o)$, where N_o is the number of shared pixels by both patches, and N_1 and N_2 are the number of pixels for the two patches that had values ≥50% of the maximum response. Patch semi-profiles are normalized responses as a function of distance from the center of the patch, obtained by radial averaging of pixel values from the patch center. Color-coded "best position maps" were calculated from single-position maps that were additionally clipped (3%), Gaussian smoothed (kernel width, 99 μm), and thresholded at >1 SD of the mean blank image value. The color of each pixel indicates the stimulus that elicited the strongest response in that pixel, whereas color saturation indicates the inverse magnitude of that response. Maps obtained from different animals were averaged after alignment by translation and rotation, such that the patches evoked by the middle two rows of stimuli (of the 6 × 4 grid) were matched best. Patch centers are the center coordinates of two-dimensional (2-D) Gaussians fitted to patches in single-position maps. The magnification factor (MF) was calculated by dividing the Euclidean distance between patch center coordinates by the difference of visual field angle (18°). Patch orientation was defined as the angle, relative to the image axes, of the major axis of the 2-D Gaussian fits of individual patches, whereas patch elongation was the ratio of the major to minor axes of those fits.

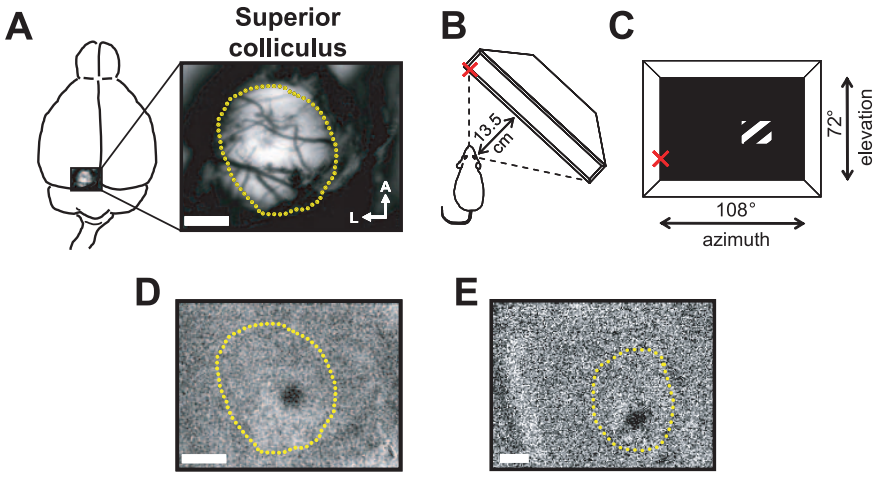

Figure 1. Intrinsic imaging of visual responses in the superior colliculus. ***A***, Dorsal view of a mouse brain depicting the location of the imaged area (left) that shows the surface of the left SC (right), exposed by aspirating the overlying cortex. The dotted line represents a rough outline of the SC. ***B***, Position of the stimulus monitor relative to the mouse, angled at 45° from the long body axis. ***C***, Schematic of monitor screen spanning ~108 × 72° (azimuth × elevation) in visual space. The stimuli were square-shaped, black/white drifting gratings presented at different locations in the visual field. The red cross marks the vertical meridian and the position of the eye in elevation. ***D***, A single position map of the contralateral SC showing a spatially restricted response (dark patch) evoked by the presentation of a 20 × 20° stimulus (average map from 12 stimulus presentations). ***E***, A single-position map of a different animal from a single, 600 ms frame. Scale bars, 0.5 mm.

Results

Imaging intrinsic signals in the SC

Previous intrinsic imaging studies in rodents have been performed in structures that lie on the surface of the brain and are thus immediately amenable to optical techniques (Masino et al., 1993; Rubin and Katz, 1999; Schuett et al., 2002). We have adapted this technique to obtain functional maps also from a deeper structure in the brain: the SC of the midbrain. After aspiration of the overlying cortex, it was possible to image intrinsic signals from the SC surface (Fig. 1*A*), evoked by visual stimulation with small patches of drifting gratings at different positions in the contralateral visual field, spanning 108° in azimuth and 72° in elevation (Fig. 1*B*,*C*), thus allowing us to acquire maps of functional retinotopy. The activity map in Figure 1*D* shows SC activation (dark patch), obtained by presenting a 20° × 20° stimulus (Fig. 1*C*) 12 times at the same position in the visual field and averaging the resulting reflectance changes of the SC surface. This "single-position" map demonstrates that the responses in the SC to individual stimuli are spatially very restricted. Intrinsic signals in the SC were also highly robust, because we could obtain maps

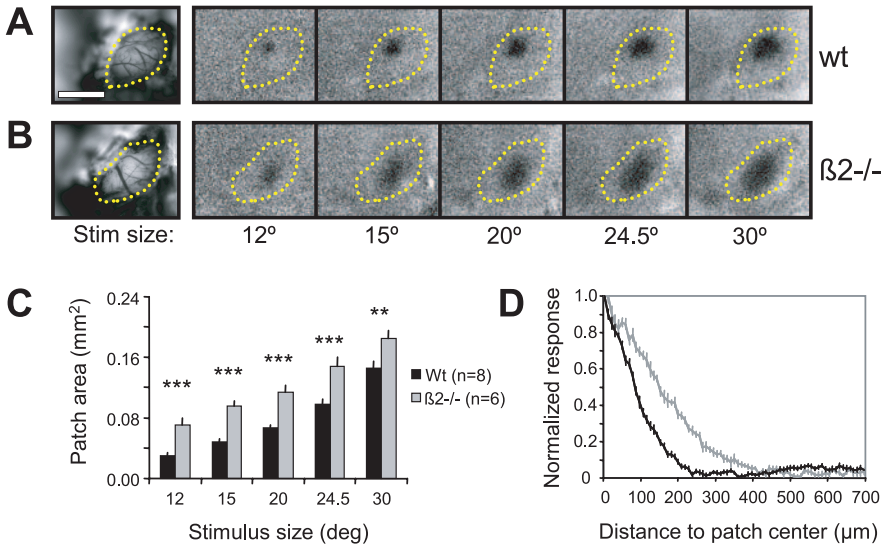

Figure 2. Stimulus representations in the SC of $\beta2^{-/-}$ mice are broader than in wt animals. ***A***, ***B***, Single-position maps obtained with five stimulus sizes (side length, 12, 15, 20, 24.5, and 30°) presented at the same position in visual space from a wt (***A***) and $\beta2^{-/-}$ (***B***) animal. The patch area increases with stimulus size, but responses in $\beta2^{-/-}$ animals are larger and blurrier for a given stimulus size. The dotted line outlines the border of the SC, which in these experiments was not exposed fully. Scale bar, 1 mm. ***C***, Quantification of the SC response area. Mean patch area values for each of the five stimulus sizes from wt and $\beta2^{-/-}$ animals. $^{**}p < 0.01$; $^{***}p < 0.001$; *t* test. ***D***, Mean, normalized semi-profiles of patches evoked by 12° stimuli in wt (black) and $\beta2^{-/-}$ (gray) animals. Note that, in $\beta2^{-/-}$ mice, there is a shallower decline of response with distance from patch center and that patch width is broader for all values below the peak response. Error bars represent SEM.

of high signal-to-noise, without averaging, from a single, 600 ms frame (Fig. 1*E*).

Stimulus mapping reveals broader activations in the SC of $\beta2^{-/-}$ mice

To assay functionally how the lack of nAChR-mediated, early retinal waves during retinotopic map refinement affects the precision of topographic mapping, we compared visually evoked responses in the SC of adult wt and $\beta2^{-/-}$ mice. For each group of animals, functional maps were obtained in response to stimuli of five different sizes presented at the same position in the visual field. An example from a wt SC is shown in Figure 2*A*. Increasing stimulus size, which activates increasingly larger regions of the retina, resulted in an enlargement of the activated SC area. Note that the borders of patches remained sharp regardless of stimulus size. Maps from $\beta2^{-/-}$ animals were similar in that they showed a stimulus size-dependent expansion of SC activation (Fig. 2*B*). The relationship between stimulus size and activated SC area (number of pixels in the patch whose values were ≥50% of the maximum reflectance change) was essentially linear in both wt and $\beta2^{-/-}$ animals (Fig. 2*C*). However, for any given stimulus size, patch area was significantly larger in $\beta2^{-/-}$ mice (Fig. 2*B*,*C*) (ANOVA, $p < 10^{-5}$). Moreover, unlike in wt mice, the patches in $\beta2^{-/-}$ animals had a blurry appearance (Fig. 2*B*), with a significantly shallower decline of response strength from the patch center to its periphery (Fig. 2*D*) (ANOVA, $p < 10^{-5}$). These results are in keeping with anatomical studies showing expanded termination zones of retinal axons in the SC of $\beta2^{-/-}$ mice (McLaughlin et al., 2003) (Chandrasekaran et al., 2005).

Given the expanded representation of stimuli in the SC of $\beta2^{-/-}$ mice, the same position in the SC should be activated by a larger region of visual field than in wt animals. We confirmed this by measuring the extent of overlap between representations of neighboring stimuli. Stimuli presented at three adjacent positions (Fig. 3*A*) (stimulus center spacing, 15°) activated neighboring regions in the SC (Fig. 3*B–E*). Keeping the center positions constant but increasing the size of stimuli resulted in more overlap between neighboring stimuli (Fig. 3*A*) and, as predicted, between their representations in the SC (Fig. 3*B–E*). The area of SC jointly activated by neighboring stimuli was indeed consistently larger in $\beta2^{-/-}$ mice (Fig. 3*F*) (ANOVA, $p < 0.001$).

One possible concern is that the larger patch sizes in $\beta2^{-/-}$ mice may arise as a consequence of increased eye movements, because it has been reported that nicotinic transmission in the monkey SC influences saccades (Watanabe et al., 2005). However, we could not detect any noticeable eye movements in anesthetized mice of either genotype. This was further confirmed by measuring the drifts of patch centers across different data acquisition blocks, and these did not differ between wt and $\beta2^{-/-}$ mice ($p = 0.56$, *t* test).

Mapping functional retinotopy in the SC

The representation of visual space in the mouse SC spans ~130° in azimuth and 90° in elevation (Dräger and Hubel, 1976). In our case, the retinotopic organization of the SC was revealed by imaging intrinsic responses to adjacent 18° × 18° stimuli that partitioned the visual field into a 6 × 4 grid (Fig. 4*B*), totaling 108° × 72°. This design ensured that each stimulus could be fully seen by the mouse and drive SC responses in its entirety. Each stimulus elicited a patch of activity that was adjacent to that evoked by a neighboring stimulus (for an example from a wt animal, see Fig. 4*C*). To illustrate the organization of the entire retinotopic map, we used a color code: each pixel in the map was assigned a color of the stimulus position (Fig. 4*B*) that had evoked the largest response at that position in the SC (Fig. 4*D*). Shifting the stimulus position from nasal to lateral visual field resulted in a posterior shift of SC activation. Similarly, increasing stimulus elevation activated more medial portions of the SC. To reveal the orderly progression of visual space across the SC surface, we constructed a map with discrete positions, by plotting the center coordinates of 2-D Gaussians fitted to patches in single-position maps (Fig. 4*E*). Retinotopic maps from other wt animals ($n = 5$) were very similar.

Gross retinotopic organization is altered in the SC of $\beta2^{-/-}$ mice

Having demonstrated that we can reliably map functional retinotopy from the surface of almost the entire SC, we measured responses in $\beta2^{-/-}$ mice to assess the effect of the elimination of retinal waves on the gross retinotopic organization (Fig. 4*F–J*). It is evident that a rough topographic order was preserved, despite larger patch sizes. However, in contrast to wt mice, the patches in the anterior SC were much more elongated along the anteroposterior (A-P) axis (Fig. 4*C*,*H*, compare *a1–d1*), resulting in a shift of their centers toward more posterior positions and a compression of the retinotopic map in the posterior half of the SC (Fig. 4*J*).

For clearer visualization and to further explore these differences in retinotopic organization, we generated maps of retinotopy from averaged single-position maps within each animal

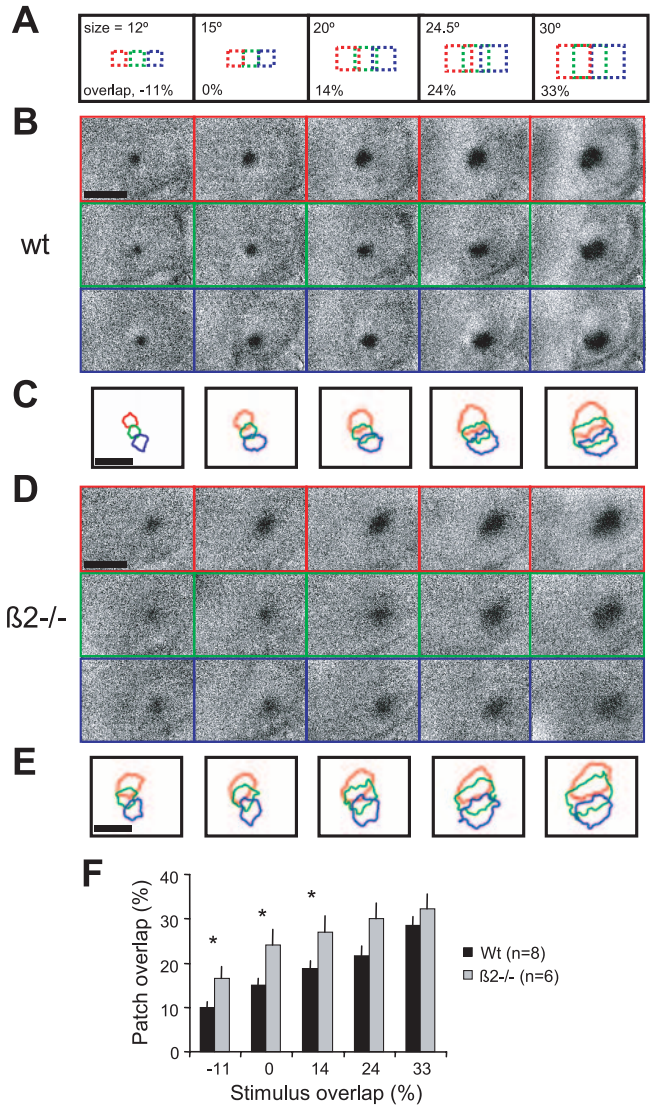

Figure 3. Responses to neighboring stimuli overlap more in $\beta2^{-/-}$ than in wt SC. ***A***, Stimulus configuration for the analysis of patch overlap. As stimulus size increases, the center positions of the three stimuli remain fixed, resulting in more overlap between adjacent stimuli. Stimulus side length and overlap are indicated. ***B***, ***D***, Single-position maps in response to stimuli depicted in ***A*** for a wt (***B***) and a $\beta2^{-/-}$ (***D***) animal. ***C***, ***E***, Colored contours circumscribe the area responding stronger than 50% of response maximum of maps shown in ***B*** and ***D***. The contour colors correspond to stimuli shown in ***A***. Note that the responses to adjacent stimuli in $\beta2^{-/-}$ animals overlap more than in wt mice regardless of stimulus size. Scale bars, 1 mm. ***F***, Quantification of SC patch overlap in wt and $\beta2^{-/-}$ animals. Patch area values for each of the five stimulus sizes averaged across wt and $\beta2^{-/-}$ animals. The spread of activity in the SC was invariably larger in $\beta2^{-/-}$ than in wt mice. The patches overlapped significantly more in $\beta2^{-/-}$ mice. Error bars represent SEM. *$p < 0.05$; *t* test.

group (Fig. 5*A*,*B*). Averaging across animals (wt, $n = 5$; $\beta2^{-/-}$, $n = 5$) was possible because the variability between retinotopic maps from different animals was very small, as indicated by the length of error bars (SD) in plots of patch center coordinates (Fig. 5*C*,*D*).

The overall retinotopic organization was quantified by the MF, a scaling factor that relates visual field angle to distance in the SC. The MF was calculated from averaged Euclidian distances between centers of patches evoked by stimuli separated by 18° either in azimuth or elevation. In both wt and $\beta2^{-/-}$ mice, the MFs were predominantly larger for stimuli separated in elevation [mediolateral (M-L) axis of SC] compared with those separated in azimuth (Fig. 5*F*,*G*), and there was a slight but significant drop in MF along the A-P SC axis (Fig. 5*F*) (ANOVA, $p < 10^{-5}$). However, whereas the MFs varied smoothly across the SC surface in wt mice (Fig. 5*C*,*F*,*G*, black symbols), the retinotopic map from $\beta2^{-/-}$ mice showed a pronounced compression of visual azimuth in the posterior part of the SC (Fig. 5*D*,*F*, gray symbols). This compression was specific for the representations of the temporal visual field (average MF for azimuths >36°, wt, 9.26 ± 0.22; $\beta2^{-/-}$, 7.07 ± 0.27 μm/°; mean ± SE; $p < 10^{-5}$, *t* test), because there was no difference in the MFs from the nasal visual field in the anterior SC between wt and $\beta2^{-/-}$ mice (average MF for azimuths <36°, wt, 11.34 ± 0.28; $\beta2^{-/-}$, 11.87 ± 0.41 μm/°; $p = 0.29$, *t* test).

There was additionally a slight but significant compression in the representation of elevation at the medial and lateral parts of the SC in $\beta2^{-/-}$ mice (Fig. 5*D*,*G*) (wt vs $\beta2^{-/-}$ MF, lateral, $p < 0.01$; medial, $p < 0.05$; *t* test). This is most likely a consequence of the anisotropy of spatial organization of projections innervating the SC borders in $\beta2^{-/-}$ mice: whereas the retinocollicular axons projecting diffusely to the central regions of the SC can extend in all directions, those targeted to the edges can arborize ectopically only toward the middle. Consequently, the "centers of mass" of patches from the medial and lateral SC borders, evoked by uppermost and lowermost stimuli, respectively, will necessarily be shifted centrally, and, as a result, the values of MFs in those regions of the SC are smaller (Fig. 5*G*).

The asymmetry in ectopic arborizations of projections targeted to SC periphery can, however, not explain the compression in the representation of azimuth along the A-P axis, because (1) there was no difference in MFs at the anterior edge of the SC between wt and $\beta2^{-/-}$ mice, and (2) the compression extended far into the SC, well away from its posterior edge. In principle, changes in magnification factor values could have arisen if the overall area or shape of SC was different between $\beta2^{-/-}$ and wt mice. However, we found no difference in the total activated area (wt, 1.57 ± 0.17; $\beta2^{-/-}$, 1.55 ± 0.15 mm^2; $n = 5$ per group; $p = 0.76$, *t* test) or aspect ratio (wt, 1.13 ± 0.04; $\beta2^{-/-}$, 1.15 ± 0.07; $n = 5$ per group; $p = 0.63$, *t* test) of SC between the two groups of animals.

Size, elongation, and orientation of response patches vary systematically along the SC

Which parameters of the retinotopic map in $\beta2^{-/-}$ mice can account for the selective compression in the representation of visual azimuth in the posterior SC? Contour plots of response patches from averaged single-position maps reveal large differences in functional topography of retinocollicular mapping between wt and $\beta2^{-/-}$ mice (Fig. 6*A*,*B*). These include changes in patch size, overlap, and shape. In both wt and $\beta2^{-/-}$ mice, patch areas were largest in the anterior SC and decreased toward its posterior end (Fig. 6*D*). Patch sizes from the $\beta2^{-/-}$ mice were invariably larger than in the wt mice (Fig. 6*D*) but without a significant change in the relative size difference along the A-P axis of the SC (Fig. 6*F*, black symbols). Patch area per se is therefore unlikely to account for the differences in the azimuthal MF. We therefore analyzed the shapes of the patches in both groups of mice by determining their elongation and orientation (Fig. 6*E*). In this plot, the length of each line represents patch elongation, defined as the aspect ratio of the major and minor axes of the 2-D Gaussians fitted to each response patch. The elongation values were largest in the anterolateral region of the SC in both wt and $\beta2^{-/-}$ mice. In $\beta2^{-/-}$ mice, however, patches were significantly more stretched out along the A-P axis (Fig. 6*E*) (mean patch aspect ratio, wt, 1.27 ± 0.02; $\beta2^{-/-}$, 1.51 ± 0.05; $p < 10^{-3}$, *t* test).

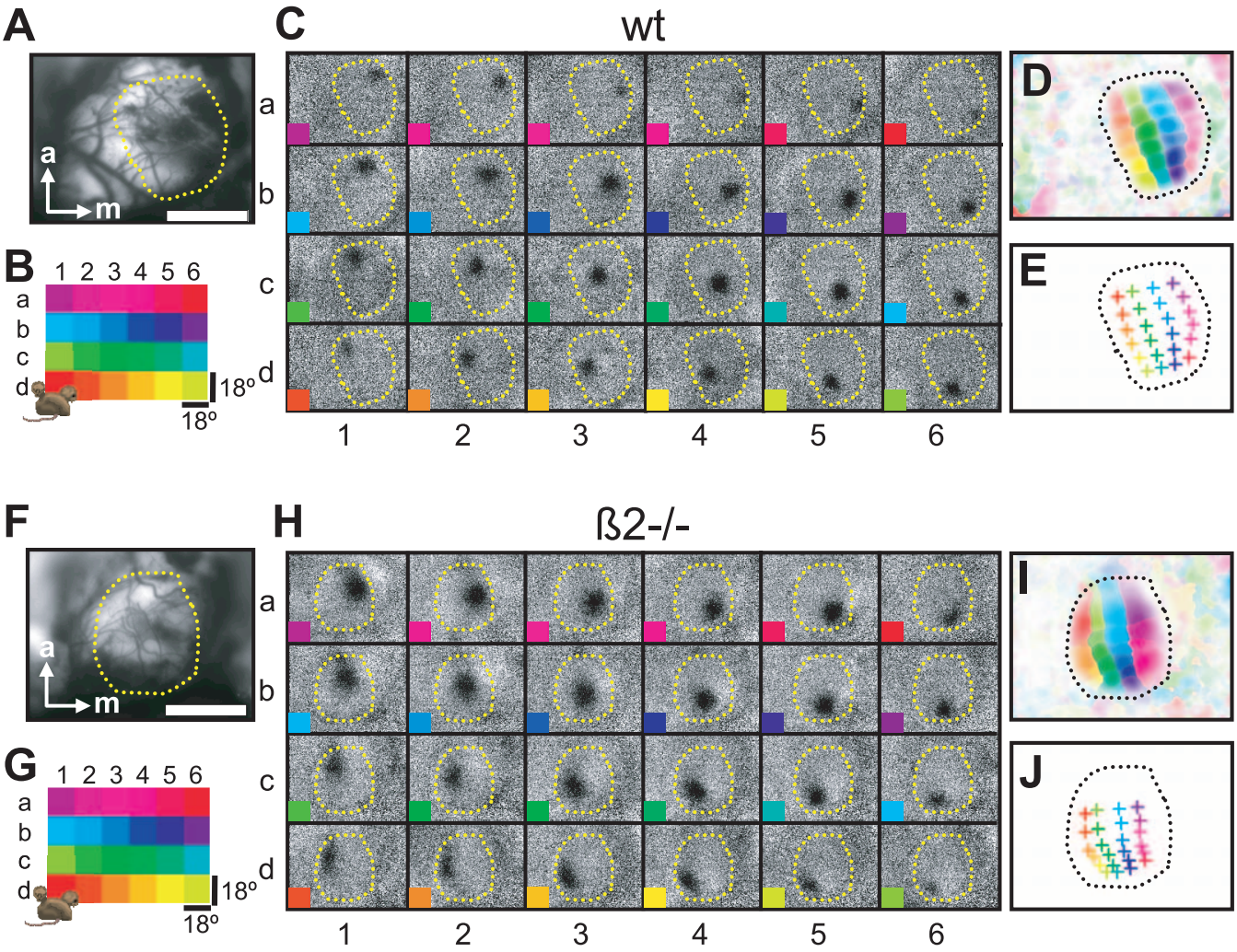

Figure 4. Mapping retinotopy in SC of wt and $\beta2^{-/-}$ mice. ***A***, ***F***, Imaged area. The dotted line represents a rough outline of the SC. Scale bars, 1 mm. ***B***, ***G***, Layout of stimuli used for mapping SC responses. Color denotes stimulus position. ***C***, ***H***, Individual activity maps showing responses (dark patches) to 24 stimulus positions as indicated by colored squares. Note that neighboring stimuli activate adjacent positions in the SC. ***D***, ***I***, Color-coded maps of overall retinotopic organization in the SC. For each pixel, color denotes the stimulus position that elicited the greatest response in that part of the SC, whereas color saturation equals the minimum intensity of all single-position maps. ***E***, ***J***, Spatial arrangement of patch centers (crosses), which are the center coordinates of 2-D Gaussians fitted to patches in single-position maps. Note the larger patches in the $\beta2^{-/-}$ mouse, as well as a pronounced compression of visual azimuth in the posterior SC.

Moreover, the differences in elongation between wt and $\beta2^{-/-}$ mice varied across the SC, being most prominent in its anterior part and rather small in the posterior part (Fig. 6*F*, gray symbols). The degree of patch elongation along the A-P axis of the SC correlated positively with MF across azimuth in $\beta2^{-/-}$ mice, whereas no such trend was apparent in the wt animals (Fig. 6*G*). Thus, the more stretched out the patch, the greater the interpatch distance along the A-P axis in the SC of $\beta2^{-/-}$ animals. These data suggest that the compression in the representation of visual azimuth in posterior SC may arise because of an increased posterior expansion of retinocollicular projections in the anterior SC.

A previous study suggested that the projection from the ipsilateral eye is more exuberant in the SC of $\beta2^{-/-}$ than in wt mice (Rossi et al., 2001). This raises the possibility that the posterior shift of patch centers in the anterior SC of $\beta2^{-/-}$ mice (Fig. 5*D*) could arise from an increased ipsilateral projection into this region. We therefore measured SC responses through either eye in response to stimulation of frontal visual space but failed to detect any ipsilaterally evoked activity in both wt ($n = 2$) and $\beta2^{-/-}$ ($n = 2$) mice (data not shown). This implies that the alterations in the topography of the contralateral eye projection take place without significant competitive influences from the ipsilateral projection.

Discussion

We used intrinsic imaging to map functionally the overall retinotopic organization of the SC in mice that lack early retinal waves. In contrast to wt mice, the representations of individual stimuli in $\beta2^{-/-}$ mice were overall larger and more elongated along the A-P axis, and there was a marked compression of visual azimuth representations in the posterior half of the SC. This compression can be explained by the anisotropy in the shape and orientation of individual stimulus representations across the A-P axis of the SC. Our results indicate that spontaneous activity in the immature retina is not only required for the local refinement of the retinotopic map but also for shaping its gross organization.

Mapping intrinsic signals in the SC

Optical imaging offers several advantages over conventional methods used for mapping the topography of retinocollicular projections. Whereas injections of anterograde anatomical tracers can at best resolve projections from very few retinal sites of set

size and microelectrode recordings are prone to sampling errors, optical imaging can be reliably used to map precisely the topography of visually evoked responses from almost the entire surface of the SC. The fact that we could resolve patches as small as ~100 μm in diameter (Fig. 2*A*) demonstrates not only the precision of retinocollicular projections but also the mapping accuracy of this method. Optical imaging is therefore ideally suited to detect both local and global changes in functional topography, which makes it a useful tool for screening mice deficient in genes important for the establishment of retinotopic maps in the SC.

Local topography is functionally less refined in $\beta2^{-/-}$ mice

Precise topography in the SC develops during the first postnatal week by large-scale remodeling of RGC axonal arbors (Simon and O'Leary, 1992; McLaughlin et al., 2003) and is thought to be regulated by retinal waves that correlate the firing of neighboring RGCs (Galli and Maffei, 1988; Meister et al., 1991; Wong et al., 1995; Bansal et al., 2000). In line with this idea, the regional topography of retinofugal projections is disrupted but not abolished in mice lacking early retinal waves, suggesting that correlated activity patterns in the retina are important primarily for retinotopic map refinement (Grubb et al., 2003; McLaughlin et al., 2003).

In this study, we provide the functional correlate of these anatomical changes by showing that a given region of the retina drives activity over a greater area of SC in $\beta2^{-/-}$ mice than in wt animals. Based on intrinsic imaging alone, one cannot distinguish whether the unrefined retinocollicular projection is accompanied by an enlargement of receptive field sizes or a large scatter of positional preferences of neurons within a given region of the SC. Recent evidence indicates that receptive field structure and size is indeed altered in $\beta2^{-/-}$ mice (Chandrasekaran et al., 2005).

There is a possibility that the disruption in remodeling of the retinocollicular projection in $\beta2^{-/-}$ mice arises from the lack of cholinergic signaling in the developing SC, especially because acetylcholine is known to be a potent modulator of synaptic transmission and plasticity (Dani, 2001). Specifically, nAChRs are expressed throughout the developing rodent brain (Naeff et al., 1992; Tribollet et al., 2004), and $\beta2$-containing nAChRs are expressed in the adult mouse SC (Marks et al., 2002). However, the developmental effects of the loss of cholinergic signaling in the SC should be minimal, because nAChR blockade with dihydro-β-erythroidine in the rat SC during the first postnatal week does not disrupt the topography of the retinocollicular projection (Simon et al., 1992). Moreover, partial topographic refinement was still observed during the first 2 postnatal weeks in the $\beta2^{-/-}$ SC (McLaughlin et al., 2003), suggesting that the capacity for developmental plasticity was maintained. We therefore consider it unlikely that the imprecise topography in $\beta2^{-/-}$ mice is caused by impaired plasticity in the SC.

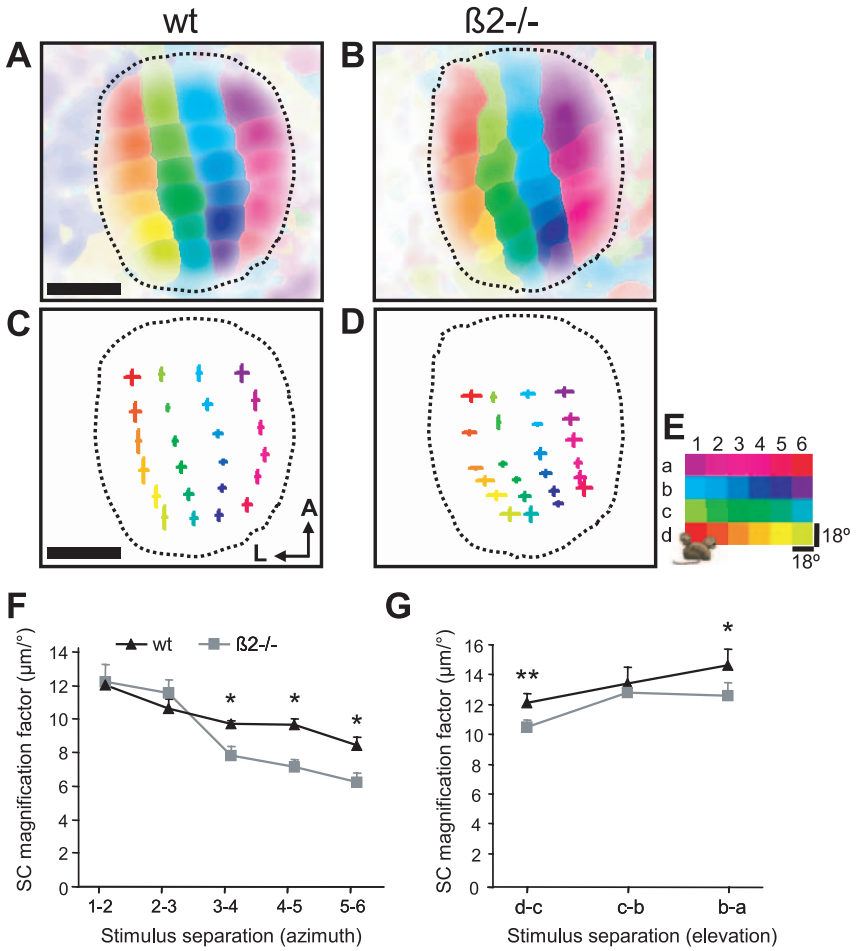

Figure 5. Overall retinotopic organization is altered in the SC of $\beta2^{-/-}$ animals. ***A***, ***B***, Averaged retinotopic maps from five wt (***A***) and five $\beta2^{-/-}$ (***B***) mice. ***C***, ***D***, Centers of patches from maps in ***A*** and ***B***. The lengths of crossing lines are the SDs of patch center coordinates in vertical and horizontal directions. Note the small variations within each experimental group as well as the compression of stimulus representation in the posterior part of the SC in $\beta2^{-/-}$ animals compared with wt animals. Color denotes stimulus position, as shown in ***E***. Scale bar, 0.5 mm. ***F***, ***G***, Quantification of SC MFs. Plots show MFs calculated from mean distances between centers of patches evoked by stimuli separated in azimuth (***F***, averaged across elevation) or in elevation (***G***, averaged across azimuth) from wt (black) and $\beta2^{-/-}$ (gray) mice. The abscissa indicates stimulus separation (always Δ18°) at different visual field positions, as indexed in ***E***. Error bars are SEM. $*p < 0.05$; $**p < 0.01$; *t* test.

Coarse retinotopy is altered in $\beta2^{-/-}$ mice

In wt animals, the visual field was mapped uniformly across the SC surface. Although neighboring stimuli still mapped to neighboring positions in the SC of $\beta2^{-/-}$ mice, the retinotopic map exhibited a posterior shift of nasal visual space and a marked compression of visual azimuth in the posterior SC.

The gross abnormalities in the retinotopic organization can be attributed to the disruptions in the precision of local topography, which were more pronounced along the A-P axis. Stimulus representations in the SC of $\beta2^{-/-}$ mice were spatially most exuberant anteriorly. Moreover, the elongated representations were oriented predominantly along the A-P axis, and there was more overlap between them along the A-P than along the M-L axis. This phenotype is a likely consequence of the way retinal axons grow into the SC at approximately the time of birth (Simon and O'Leary, 1992; McLaughlin et al., 2003). First, there is a bias in the anatomical order of the ingrowing optic tract fibers, which seem to be initially more ordered along the M-L than in the A-P axis of the SC (Simon and O'Leary, 1991, 1992; McLaughlin et al., 2003).

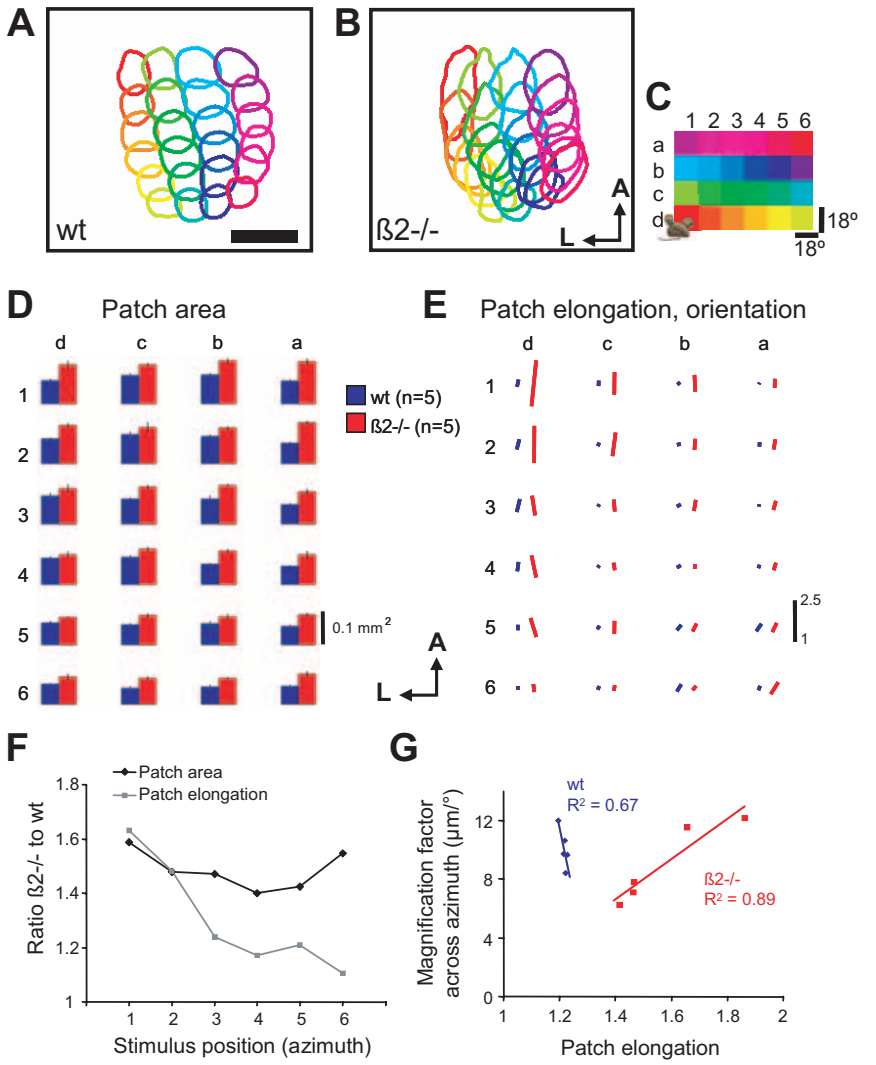

Figure 6. More elongated response patches in the SC of $\beta2^{-/-}$ mice can account for the changes in retinotopic map organization. ***A***, ***B***, Colored contours of averaged retinotopic maps (from Fig. 5*A*, *B*) circumscribe a patch area that is ≥65% of response maximum (65% contour is used here only for clearer visualization). ***D***, Area of SC activated by stimulation at different positions. The values represent average patch areas corresponding to ≥50% of response maximum from five wt (blue) and five $\beta2^{-/-}$ (red) mice. Stimulus position corresponds to indices in ***C***. Error bars are SEM. ***E***, Patch aspect ratio and orientation for each stimulus position, as indexed in ***C***. The line length is the aspect ratio of the major and minor axes of the 2-D Gaussians fitted to each patch (i.e., a value of 1 indicates a round patch). The line tilt represents patch orientation relative to image axes. Note that patches from $\beta2^{-/-}$ mice are stretched along the anteroposterior axis of the SC. ***F***, Ratios ($\beta2^{-/-}$/wt) of mean area (black) and elongation (gray) values from patches evoked by stimuli separated in azimuth (as indexed in ***C***) and averaged across elevation. Note here that, relative to wt mice, the patches from $\beta2^{-/-}$ mice are much longer in the anterior SC than more posteriorly. ***G***, MF values of visual azimuth (from Fig. 5*F*) plotted against patch elongation for wt (blue) and $\beta2^{-/-}$ (red) mice from the equivalent positions in the SC. There was a positive correlation between MF and patch length ($R^2 = 0.89$) in the $\beta2^{-/-}$ animals, whereas there was no such correlation for wt animals.

The lack of retinal waves in $\beta2^{-/-}$ mice during the first postnatal week, which prevents refinement, may accentuate the differences in the initial mapping precision between the two SC axes. Second, during the remodeling period, the overall degree of retraction that eliminates inappropriately targeted arborizations appears to be greater for projections from the temporal retina, which innervate the anterior SC, because overshooting axons and their branches have to be withdrawn from a far larger area than for those from the nasal retina (Simon and O'Leary, 1992). In effect, the lack of correlated activity patterns in the retina, which mediate the retraction of ectopic arborizations, may result in a relatively greater elongation of stimulus representations in the anterior SC than of those more posteriorly.

Our explanation, then, of why the retinotopic map is compressed posteriorly in $\beta2^{-/-}$ mice is based on the following reasoning. Because of the lack of retinal waves during the first postnatal week, the temporal RGC axons targeted to the anterior SC preferentially maintain their ectopic branches more posteriorly, in which these can compete for postsynaptic neurons with axons projecting from more nasal portions of the retina. This results in the posterior shift of the center of mass of stimulus representations from the anterior SC. In contrast, at the posterior end of the SC, the projections from the nasal retina are not nearly as large or elongated, and do not invade, and therefore cannot compete for postsynaptic target space more anteriorly. The net result is both a shift in the representation of nasal visual space more posteriorly and a compression in the representation of visual azimuth in the remaining, posterior part of the SC in $\beta2^{-/-}$ mice. Therefore, the deficit in the local topographic refinement that arises from the lack of early correlated activity in the retina, in combination with the orientated ingrowth of RGC axons, could lead to general changes in the retinotopic map layout.

General implications for activity-dependent map formation

Previous studies using TTX or genetic manipulations to block retinal ganglion cell firing also showed that neuronal activity alters retinotectal mapping (Thompson and Holt, 1989; Gnuegge et al., 2001). However, these studies could not distinguish between a permissive role, whereby neuronal activity merely permits axons to respond to molecular cues, or an instructive one, whereby the spatiotemporal pattern of neuronal activity determines topographic order, most likely by elimination of inappropriately connected axons (Ruthazer et al., 2003). Because the $\beta2^{-/-}$ mice differ from wt animals only in the spatiotemporal pattern of retinal ganglion cell firing, without a significant reduction in overall activity levels, our data in conjunction with the anatomical data in the SC of $\beta2^{-/-}$ mice (McLaughlin et al., 2003) show that neuronal activity has an instructive function in retinotopic mapping.

Whereas the results from this and previous studies have demonstrated that patterned activity in the retina is essential for regional refinement of topography in retinal targets (Grubb et al., 2003; McLaughlin et al., 2003), our results also stress the requirement of correlated retinal activity in shaping the gross retinotopic map structure in the SC. The marked distortion of both fine-scale (this study) (Grubb et al., 2003) and coarse (this study) retinotopy along the nasotemporal axis in targets of retinal projections in $\beta2^{-/-}$ mice indicates that early retinal waves have a greater

role than previously thought in the specification of retinotopic order, at least along one visual axis.

The importance of patterned retinal activity has also been demonstrated for the segregation of RGC axons into eye-specific domains in the LGN (Rossi et al., 2001; Stellwagen and Shatz, 2002; Torborg et al., 2005) (but see Huberman et al., 2003), suggesting that similar activity-dependent mechanisms may guide the formation of both eye-specific connections and precise topographic maps during early postnatal development. Thus, at several stages of the mammalian nervous system, the specific pattern of neuronal activity is instructive in shaping the structure of functional maps.

References

Bansal A, Singer JH, Hwang BJ, Xu W, Beaudet A, Feller MB (2000) Mice lacking specific nicotinic acetylcholine receptor subunits exhibit dramatically altered spontaneous activity patterns and reveal a limited role for retinal waves in forming ON and OFF circuits in the inner retina. J Neurosci 20:7672–7681.

Bonhoeffer F, Huf J (1982) In vitro experiments on axon guidance demonstrating an anterior-posterior gradient on the tectum. EMBO J 1:427–431.

Bonhoeffer T, Grinvald A (1996) Optical imaging based on intrinsic signals: the methodology. In: Brain mapping: the methods (Toga AW, Mazziotta JC, eds), pp 55–97. San Diego: Academic.

Butts DA (2002) Retinal waves: implications for synaptic learning rules during development. The Neuroscientist 8:243–253.

Chandrasekaran AR, Plas DT, Gonzalez E, Crair MC (2005) Evidence for an instructive role of retinal activity in retinotopic map refinement in the superior colliculus of the mouse. J Neurosci 25:6929–6938.

Changeux JP, Danchin A (1976) Selective stabilisation of developing synapses as a mechanism for the specification of neuronal networks. Nature 264:705–712.

Cheng HJ, Nakamoto M, Bergemann AD, Flanagan JG (1995) Complementary gradients in expression and binding of ELF-1 and Mek4 in development of the topographic retinotectal projection map. Cell 82:371–381.

Cline HT, Constantine-Paton M (1989) NMDA receptor antagonists disrupt the retinotectal topographic map. Neuron 3:413–426.

Dani JA (2001) Overview of nicotinic receptors and their roles in the central nervous system. Biol Psychiatry 49:166–174.

Dräger UC, Hubel DH (1976) Topography of visual and somatosensory projections to mouse superior colliculus. J Neurophysiol 39:91–101.

Drescher U, Kremoser C, Handwerker C, Loschinger J, Noda M, Bonhoeffer F (1995) In vitro guidance of retinal ganglion cell axons by RAGS, a 25 kDa tectal protein related to ligands for Eph receptor tyrosine kinases. Cell 82:359–370.

Feldheim DA, Kim YI, Bergemann AD, Frisen J, Barbacid M, Flanagan JG (2000) Genetic analysis of ephrin-A2 and ephrin-A5 shows their requirement in multiple aspects of retinocollicular mapping. Neuron 25:563–574.

Feller MB (2002) The role of nAChR-mediated spontaneous retinal activity in visual system development. J Neurobiol 53:556–567.

Frisen J, Yates PA, McLaughlin T, Friedman GC, O'Leary DD, Barbacid N (1998) Ephrin-A5 (AL-1/RAGS) is essential for proper retinal axon guidance and topographic mapping in the mammalian visual system. Neuron 20:235–243.

Galli L, Maffei L (1988) Spontaneous impulse activity of rat retinal ganglion cells in prenatal life. Science 242:90–91.

Gnuegge L, Schmid S, Neuhauss SC (2001) Analysis of the activity-deprived zebrafish mutant macho reveals an essential requirement of neuronal activity for the development of a fine-grained visuotopic map. J Neurosci 21:3542–3548.

Grinvald A, Lieke E, Frostig RD, Gilbert CD, Wiesel TN (1986) Functional architecture of cortex revealed by optical imaging of intrinsic signals. Nature 324:361–364.

Grubb MS, Rossi FM, Changeux JP, Thompson ID (2003) Abnormal functional organization in the dorsal lateral geniculate nucleus of mice lacking the beta 2 subunit of the nicotinic acetylcholine receptor. Neuron 40:1161–1172.

Hindges R, McLaughlin T, Genoud N, Henkemeyer M, O'Leary DD (2002) EphB forward signaling controls directional branch extension and arborization required for dorsal-ventral retinotopic mapping. Neuron 35:475–487.

Huberman AD, Wang GY, Liets LC, Collins OA, Chapman B, Chalupa LM (2003) Eye-specific retinogeniculate segregation independent of normal neuronal activity. Science 300:994–998.

Kalatsky VA, Stryker MP (2003) New paradigm for optical imaging: temporally encoded maps of intrinsic signal. Neuron 38:529–545.

Marks MJ, Whiteaker P, Grady SR, Picciotto MR, McIntosh JM, Collins AC (2002) Characterization of [(125)I]epibatidine binding and nicotinic agonist-mediated (86) Rb(+) efflux in interpeduncular nucleus and inferior colliculus of beta2 null mutant mice. J Neurochem 81:1102–1115.

Masino SA, Kwon MC, Dory Y, Frostig RD (1993) Characterization of functional organization within rat barrel cortex using intrinsic signal optical imaging through a thinned skull. Proc Natl Acad Sci USA 90:9998–10002.

McLaughlin T, Torborg CL, Feller MB, O'Leary DD (2003) Retinotopic map refinement requires spontaneous retinal waves during a brief critical period of development. Neuron 40:1147–1160.

Meister M, Wong RO, Baylor DA, Shatz CJ (1991) Synchronous bursts of action potentials in ganglion cells of the developing mammalian retina. Science 252:939–943.

Mrsic-Flogel T, Hubener M, Bonhoeffer T (2003) Brain mapping: new wave optical imaging. Curr Biol 13:R778–R780.

Naeff B, Schlumpf M, Lichtensteiger W (1992) Pre- and postnatal development of high-affinity [^{3}H]nicotine binding sites in rat brain regions: an autoradiographic study. Brain Res Dev Brain Res 68:163–174.

Picciotto MR, Zoli M, Lena C, Bessis A, Lallemand Y, Le Novere N, Vincent P, Pich EM, Brulet P, Changeux JP (1995) Abnormal avoidance learning in mice lacking functional high-affinity nicotine receptor in the brain. Nature 374:65–67.

Rossi FM, Pizzorusso T, Porciatti V, Marubio LM, Maffei L, Changeux JP (2001) Requirement of the nicotinic acetylcholine receptor beta 2 subunit for the anatomical and functional development of the visual system. Proc Natl Acad Sci USA 98:6453–6458.

Rubin BD, Katz LC (1999) Optical imaging of odorant representations in the mammalian olfactory bulb. Neuron 23:499–511.

Ruthazer ES, Akerman CJ, Cline HT (2003) Control of axon branch dynamics by correlated activity in vivo. Science 301:66–70.

Schuett S, Bonhoeffer T, Hubener M (2002) Mapping retinotopic structure in mouse visual cortex with optical imaging. J Neurosci 22:6549–6559.

Simon DK, O'Leary DD (1991) Relationship of retinotopic ordering of axons in the optic pathway to the formation of visual maps in central targets. J Comp Neurol 307:393–404.

Simon DK, O'Leary DD (1992) Development of topographic order in the mammalian retinocollicular projection. J Neurosci 12:1212–1232.

Simon DK, Prusky GT, O'Leary DD, Constantine-Paton M (1992) *N*-methyl-D-aspartate receptor antagonists disrupt the formation of a mammalian neural map. Proc Natl Acad Sci USA 89:10593–10597.

Sperry R (1963) Chemoaffinity in the orderly growth of nerve fiber patterns and connections. Proc Natl Acad Sci USA 50:703–710.

Stellwagen D, Shatz CJ (2002) An instructive role for retinal waves in the development of retinogeniculate connectivity. Neuron 33:357–367.

Thompson I, Holt C (1989) Effects of intraocular tetrodotoxin on the development of the retinocollicular pathway in the Syrian hamster. J Comp Neurol 282:371–388.

Torborg CL, Hansen KA, Feller MB (2005) High frequency, synchronized bursting drives eye-specific segregation of retinogeniculate projections. Nat Neurosci 8:72–78.

Tribollet E, Bertrand D, Marguerat A, Raggenbass M (2004) Comparative distribution of nicotinic receptor subtypes during development, adulthood and aging: an autoradiographic study in the rat brain. Neuroscience 124:405–420.

Watanabe M, Kobayashi Y, Inoue Y, Isa T (2005) Effects of local nicotinic activation of the superior colliculus on saccades in monkeys. J Neurophysiol 93:519–534.

Willshaw DJ, von der Malsburg C (1976) How patterned neural connections can be set up by self-organization. Proc R Soc Lond B Biol Sci 194:431–445.

Wong RO (1999) Retinal waves and visual system development. Annu Rev Neurosci 22:29–47.

Wong RO, Chernjavsky A, Smith SJ, Shatz CJ (1995) Early functional neural networks in the developing retina. Nature 374:716–718.

Wong WT, Myhr KL, Miller ED, Wong RO (2000) Developmental changes in the neurotransmitter regulation of correlated spontaneous retinal activity. J Neurosci 20:351–360.

Xu W, Orr-Urtreger A, Nigro F, Gelber S, Sutcliffe CB, Armstrong D, Patrick JW, Role LW, Beaudet AL, De Biasi M (1999) Multiorgan autonomic dysfunction in mice lacking the β2 and the β4 subunits of neuronal nicotinic acetylcholine receptors. J Neurosci 19:9298–9305.

Zhou ZJ, Zhao D (2000) Coordinated transitions in neurotransmitter systems for the initiation and propagation of spontaneous retinal waves. J Neurosci 20:6570–6577.